Research Article Vol. 41, No. 4 / April 2024 / Journal of the Optical Society of America B 1031

Journal of the Optical Society of America B

OPTICAL PHYSICS

Generalized Bloch boundary conditions based on a symmorphic space group and the finite-element implementation in photonic crystal

JINGWEI WANG,[1] LIDA LIU,[1] ZHANWEN WANG,[1] YUHAO JING,[1] AND YUNTIAN CHEN[1,2,3,*]

[1]School of Optical and Electronic Information, Huazhong University of Science and Technology, Wuhan 430074, China
[2]Wuhan National Laboratory of Optoelectronics, Huazhong University of Science and Technology, Wuhan 430074, China
[3]Optics Valley Laboratory, Wuhan 430074, China
*yuntian@hust.edu.cn

Received 8 December 2023; revised 14 February 2024; accepted 14 February 2024; posted 13 March 2024; published 25 March 2024

We studied generalized Bloch boundary conditions and their finite element implementation within the theoretical framework of a symmorphic space group. By combining translation symmetry operations with mirror and rotational symmetry operations, we developed a procedure for implementing generalized Bloch boundary conditions in the finite element method (FEM) for periodic photonic structures. First, we lay out the theoretical foundation and numerical implementation of generalized Bloch boundary conditions in FEM. We illustrate the proposed method via 2D/3D periodic photonic structures. Without a loss of generality, we calculate the band structures of 2D/3D photonic crystals using our proposed generalized Bloch boundary conditions and benchmark the results against the conventional Bloch boundary conditions. The comparisons show that band structure and eigenmode yield excellent agreement with the results obtained from conventional Bloch boundary conditions. However, our method has improved the computational efficiency by at least twofold. We further elaborate the comparisons with computation errors, memory efficiency, and computation times, all of which show that our proposed method outperforms the conventional one due to careful consideration of the mirror and rotational symmetry operation, apart from the translation symmetry. In addition, our method can easily be extended to other methods such as FDTD and transfer matrix.

https://doi.org/10.1364/JOSAB.514857

1. INTRODUCTION

Symmetry plays an indispensable role in physics, as well as in numerical computation, especially in the field of computational photonics. Properly treating the symmetry properties of photonic structures is a routine procedure to simplify computational problems and lower the computation load. For instance, perfect electric conductor (PEC) and perfect magnetic conductor (PMC) conditions can be utilized to truncate domains for mirror-symmetric devices [1–6]. The eigenmode problems of infinitely long waveguides can be reduced to a two-dimensional problem using the principle of continuous translation symmetry. When dealing with the eigenmode problems of the rotationally symmetric waveguides [7–9], only the calculation of the rotational unit is necessary when implementing the rotational Bloch boundary conditions. Similarly, for the eigenproblem of periodic crystals, utilizing the Bloch boundary conditions can reduce the computation domains to the primitive cell [10–15].

Photonic crystals [16,17] are a type of typical periodic photonic structures. The photonic band gap formed by their periodic structure can not only control the propagation of light but also exhibit topological phenomena. With the development of the band theory and wave function of photonic crystals, including investigations involving bound states in the continuum [18–22], topological insulators [23–26], and valley photonic crystals [27–29], photonic crystals have led to the development of increasingly complex structures. Despite significant efforts to apply symmetry principles to the eigenfunction problems of periodic photonic structures, to the best of our knowledge, a comprehensive treatment of computing photonic crystal structures is still lacking. Commonly, utilizing the Bloch boundary conditions obtained from discrete translational symmetry [30], other symmetries associated with unit cell that can further reduce the computation domain are often neglected. This is because the space group symmetry fully accounts for the periodic photonic structure, which contains the translation, rotation, mirror, glide, and screw symmetry or combinations. It is challenging to include translation symmetry operations and other symmetry simultaneously due to the symmetry of the device; in addition, that of the eigenmodes it possesses are not entirely consistent as different eigenmodes may only satisfy part of the symmetry. For instance, the symmetry of the eigenmodes

in a photonic crystal does not extend beyond the symmetry of the device itself, and the symmetry of the eigenmodes at different k points may not be entirely identical. Furthermore, even if they possess the exact symmetry, eigenmodes belonging to different categories may still exhibit different manifestations. For example, in a mirror-symmetric device, all eigenmodes exhibit mirror symmetry, but the eigenmodes concerning the mirror axis can either be mirror-symmetric or anti-symmetric.

In this paper, we conceive the generalized Bloch boundary conditions that combine different symmetries and their application to the FEM calculation of the band structures of photonic crystals. Group theory extends the Bloch boundary conditions to obtain the generalized Bloch boundary conditions for the symmorphic space group, resulting in a more compact calculation domain and enhanced computational efficiency. This paper has a total of four sections. Section 2 presents the derivation process of the generalized Bloch boundary conditions and elaborates on its application using mirror symmetry and rotational symmetry, resulting in the mirror Bloch boundary conditions and rotational Bloch boundary conditions. In Section 3, we compute the photonic crystal's eigenmodes at its highly symmetric point and its band structures on the highly symmetric line. Two-dimensional and three-dimensional photonic crystal examples are employed as evidence of the universal and efficient nature of the method proposed in this paper. Finally, the conclusion is reached in Section 4.

2. THEORETICAL FORMULATIONS AND NUMERICAL IMPLEMENTATIONS

Consider a crystal with the space group G, where its group element is $\{R|\boldsymbol{R}_n\}$. The lattice vector of the photonic crystal is $\boldsymbol{R}_n = \hat{x}a_1n_1 + \hat{y}a_2n_2 + \hat{z}a_3n_3$, where $n_1/n_2/n_3$ are integers. The group formed by the set of operators $\{R|0\}$ is called the point group G_0 of the space group G, which includes the rotation and mirror symmetry operations [30]. If R is an operation in G_0, where $R\boldsymbol{k} = \boldsymbol{k} + \boldsymbol{G}_h$, $\boldsymbol{G}_h$ is the reciprocal lattice vector. The collection of all Rs is called the wave vector group $G_0(\boldsymbol{k})$. Clearly, $G_0(\boldsymbol{k})$ is a subgroup of G_0.

If both the translational group $\{E|\boldsymbol{R}_n\}$ and point group G_0 are subgroups of space group G, the space group G is coined as symmorphic space group. If G_0 is not a subgroup of G, the space group is called the non-symmorphic space group. The $G_0(\boldsymbol{k})$ of the symmorphic space group contains only mirror and rotational symmetry operations. In the following, we discuss the general considerations and practical finite element implementation of calculating the eigenmode of the photonic crystals with symmorphic space group symmetry. Photonic crystals with non-symmorphic space groups, though equally important from a computational perspective, are more complex and beyond the scope of this paper.

A. General Considerations

According to the Bloch theorem, the eigenmode of a photonic crystal takes the form of the Bloch function, $\boldsymbol{\psi}^{\boldsymbol{k}}(\boldsymbol{r}) = e^{i\boldsymbol{k}\cdot\boldsymbol{r}}\boldsymbol{u}^{\boldsymbol{k}}(\boldsymbol{r})$, where $\boldsymbol{k} = \hat{x}k_x + \hat{y}k_y + \hat{z}k_z$ represents the wave vector, $\boldsymbol{r}$ denotes the spatial coordinate, and $\boldsymbol{u}^{\boldsymbol{k}}(\boldsymbol{r})$ is a periodic function that satisfies $\boldsymbol{u}^{\boldsymbol{k}}(\boldsymbol{r}) = \boldsymbol{u}^{\boldsymbol{k}}(\boldsymbol{r} + \boldsymbol{R}_n)$. The Bloch boundary condition can be expressed as

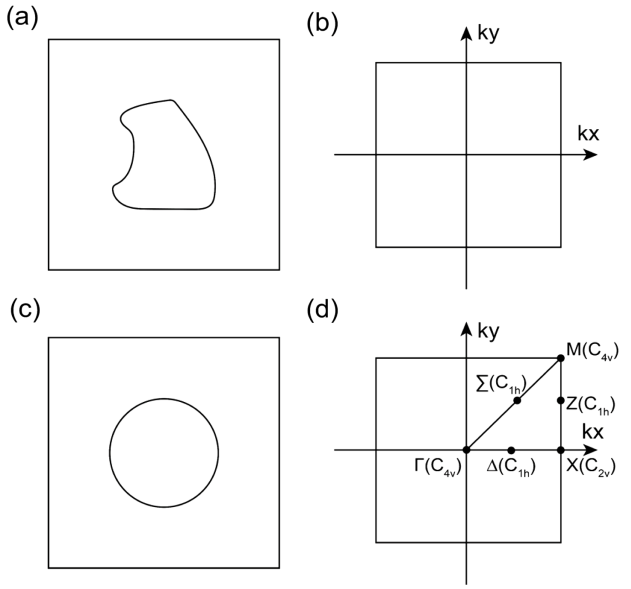

Fig. 1. Square lattices with different symmetry. (a) Square lattice without any symmetry in its unit cell. (b) Brillouin zone of (a). (c) Square lattice with $C_{4,v}$ symmetry in its unit cell. (d) Highly symmetric points or lines inside the Brillouin zone of (c).

$$\boldsymbol{\psi}^{\boldsymbol{k}}(\boldsymbol{r}) = e^{i\boldsymbol{k}\cdot\boldsymbol{R}_n}\boldsymbol{\psi}^{\boldsymbol{k}}(\boldsymbol{r} + \boldsymbol{R}_n). \tag{1}$$

Equation (1) is derived from the translational group $\{E|\boldsymbol{R}_n\}$ of the photonic crystals. As an example, Fig. 1(a) represents a unit cell of a two-dimensional photonic crystal, and the eigenmodes of the photonic crystal can be calculated by applying the Bloch boundary conditions in Eq. (1). Notably, there is no additional symmetry for the unit cell shown in Fig. 1(a); therefore, there are no highly symmetric points in the Brillouin zone, as shown in Fig. 1(b).

In contrast, if the unit cell possesses symmetry by itself, the eigenmode also exhibits symmetry at highly symmetric points A photonic crystal with $C_{4,v}$ symmetry can be seen in Figs. 1(c) and 1(d). Accordingly, the computational domain can be further truncated by taking the symmetric properties of eigenmode at those highly symmetric points/lines, as shown in Fig. 1(d). Indeed, the eigenmodes of photonic devices with symmorphic space group symmetry do not necessarily satisfy all symmetries in G_0, but they do satisfy all symmetry in $G_0(\boldsymbol{k})$ [30]. Therefore, the symmetry operation $R_k \in G_0(\boldsymbol{k})$ performed on the eigenmode yields

$$P(R_k)\boldsymbol{\psi}^{\boldsymbol{k}}(\boldsymbol{r}) = \hat{R}_k\boldsymbol{\psi}^{\boldsymbol{k}}\left(\hat{R}_k^{-1}\boldsymbol{r}\right) = \chi(R_k)\boldsymbol{\psi}^{\boldsymbol{k}}(\mathbf{r}), \tag{2}$$

where $P(R_k)/\hat{R}_k/\chi(R_k)$ represents the operator/matrix/character associated with the symmetry operation R_k. The matrix $\hat{R}_k$ corresponding to the rotational symmetry C_N around the z axis rotation is $R_z(\theta) = \begin{pmatrix} \cos\theta & -\sin\theta & 0 \\ \sin\theta & \cos\theta & 0 \\ 0 & 0 & 1 \end{pmatrix}$, and the matrix $\hat{R}_k$ corresponding to mirror symmetry σ_v is $S_z(\theta) = \begin{pmatrix} \cos 2\theta & \sin 2\theta & 0 \\ \sin 2\theta & -\cos 2\theta & 0 \\ 0 & 0 & 1 \end{pmatrix}$. Combining Eqs. (1) and (2),

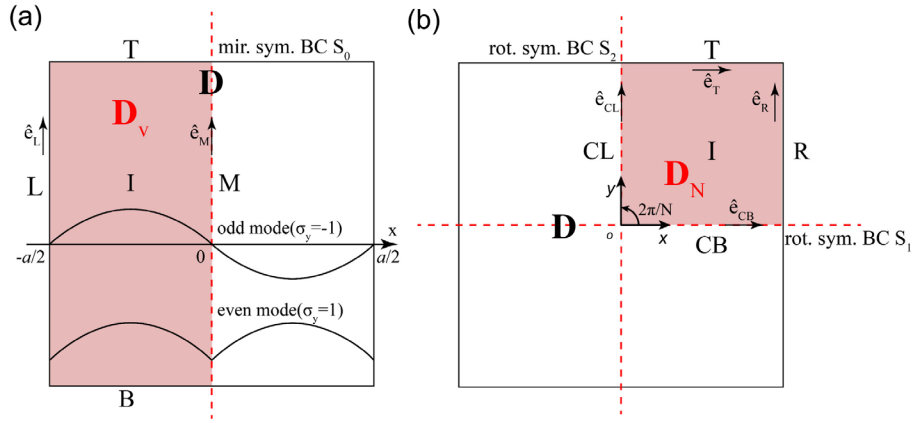

Fig. 2. Periodic unit cell with symmetry: (a) mirror symmetry and (b) rotation symmetry.

leads to the relation

$$\hat{R}_k \boldsymbol{\psi}^{\boldsymbol{k}}\left(\hat{R}_k^{-1}\boldsymbol{r}\right) = \chi(R_k) e^{i\boldsymbol{k}\cdot\boldsymbol{R}_n} \boldsymbol{\psi}^{\boldsymbol{k}}(\boldsymbol{r}+\boldsymbol{R}_n). \tag{3}$$

Equation (3) represents the generalized Bloch boundary conditions, which permits the use of a smaller computational domain than that equipped with the Bloch boundary conditions defined in Eq. (1). When $R_k = E$, Eq. (3) degenerates into the Bloch boundary conditions, and when $\boldsymbol{k} = 0$, Eq. (3) degenerates into purely symmetric boundary conditions for R_k. The $G_0(k)$ at the highly symmetric k points in Fig. 1(d) contains symmetries in addition to the null operation E. At these k points, the eigenmodes possess mirror or rotational symmetries, which are the very problem that we intend to solve in this paper. To illustrate the basic idea of a generalized Bloch boundary, we consider two photonic crystals that contain mirror symmetry and rotation symmetry in their unit cells, respectively.

B. Mirror and Rotation Symmetry

First, we consider the unit cell of a photonic crystal in which the mirror symmetry operation σ_y (mirror axis M) with respect to $k_x = 0$ exists, as shown in Fig. 2(a). We define the calculation domain using the Bloch boundary conditions as D, whereas the calculation domain for our method is represented as D_v. $\hat{e}_L/\hat{e}_M$ represents the unit tangent vector on boundary L/M. The boundaries of D_v consist of four parts: T, B, L, and M. The boundary degrees of freedom (DOFs) of FEM that are designated as u are reorganized into the following four groups: upper, upper-left, upper-right, and mirror axis, with subscripts u_T, u_B, u_L, u_M, respectively. From Eq. (1), one can have $\boldsymbol{\psi}^{\boldsymbol{k}}(T) = e^{ik_y a_2}\boldsymbol{\psi}^{\boldsymbol{k}}(B)$, which indicates that the T and B boundaries obey the Bloch boundary conditions. Therefore, we can get

$$u_T = e^{ik_y a_2} u_B. \tag{4}$$

According to Eq. (3), when $R_k = \sigma_y$, $R_n = -a\hat{x}$, $r = \frac{a}{2}\hat{x} + y\hat{y}$, and $S_z(\frac{\pi}{2}) = \begin{pmatrix} -1 & 0 & 0 \\ 0 & 1 & 0 \\ 0 & 0 & 1 \end{pmatrix}$, we can get $\hat{e}_L \cdot \boldsymbol{\psi}_t^{\boldsymbol{k}}(L) = \chi(\sigma_y)\hat{e}_L \cdot \boldsymbol{\psi}_t^{\boldsymbol{k}}(L)$ and $\psi_z^k(L) = \chi(\sigma_y)\psi_z^k(L)$, where subscript t/z represents the transverse/longitudinal components of the electric field. Similarly, when $R_k = \sigma_y$, $R_n = 0$, and $r = y\hat{y}$, we can get $\hat{e}_M \cdot \boldsymbol{\psi}_t^{\boldsymbol{k}}(M) = \chi(\sigma_y)\hat{e}_M \cdot \boldsymbol{\psi}_t^{\boldsymbol{k}}(M)$ and $\psi_z^k(M) = \chi(\sigma_y)\psi_z^k(M)$. Finally, we get [7]

$$\begin{bmatrix} u_L \\ u_M \end{bmatrix} = \begin{bmatrix} \chi(\sigma_y) & 0 \\ 0 & \chi(\sigma_y) \end{bmatrix} \begin{bmatrix} u_L \\ u_M \end{bmatrix}, \tag{5}$$

where the character $\chi(\sigma_y)$ can only be chosen as either $+1$ or -1. The L and M boundary conditions are dependent on the value of $\chi(\sigma_y)$. The DOFs at L and M are unconstrained when $\chi(\sigma_y) = 1$, $u_L = u_L$, and $u_M = u_M$. The generalized Bloch boundary conditions are reduced to PMC in this situation. However, if $\chi(\sigma_y) = -1$, $u_T = 0$, and $u_M = 0$, the boundary conditions are simplified to PEC. It is worth noting that since $k_x = 0$ is chosen, the translation symmetry in the x direction does not affect the electric field, so the generalized Bloch boundary conditions degenerate into the mirror symmetric boundary conditions. As for computing the band structures of photonic crystals, the two cases ($\chi(\sigma_y) = 1$ and $\chi(\sigma_y) = -1$) both will be accounted for to recover the full bands. The boundary conditions obtained by combining translation symmetry with mirror symmetry are referred to as mirror Bloch boundary conditions in this paper.

Second, as shown in Fig. 2(b), we consider the rotational symmetry operation c_N applied upon the calculation domain (D_N), where o is the rotational center. $\hat{e}_T/\hat{e}_R/\hat{e}_{\mathrm{CB}}/\hat{e}_{\mathrm{CL}}$ represents the unit tangent vector on boundary $T/R/\mathrm{CB}/\mathrm{CL}$. The boundary DOFs are reorganized as upper-right, right-upper, left rotational axis, bottom rotational axis, and the interior, indicated by $u_T, u_R, u_{\mathrm{CL}}, u_{\mathrm{CB}}$ and u_I respectively, where the subscripts T, R, CB, and CL denote the four corresponding boundary segments. From Eq. (3), we can get $\hat{e}_{\mathrm{CB}} \cdot \boldsymbol{\psi}_t^{\boldsymbol{k}}(\mathrm{CB}) = \chi(c_N)\hat{e}_{\mathrm{CL}} \cdot \boldsymbol{\psi}_t^{\boldsymbol{k}}(\mathrm{CL})$, $\psi_z^k(\mathrm{CB}) = \chi(c_N)\psi_z^k(\mathrm{CL})$, $\hat{e}_T \cdot \boldsymbol{\psi}_t^{\boldsymbol{k}}(T) = \chi(c_N)e^{ik_x a_1}\hat{e}_R \cdot \boldsymbol{\psi}_t^{\boldsymbol{k}}(R)$ and $\psi_z^k(T) = \chi(c_N)\psi_z^k(R)$. Finally, we get

$$\begin{bmatrix} u_{\mathrm{CB}} \\ u_T \end{bmatrix} = \begin{bmatrix} \chi(c_N) & 0 \\ 0 & \chi(c_N)e^{ik_x a_1} \end{bmatrix} \begin{bmatrix} u_{\mathrm{CL}} \\ u_R \end{bmatrix}, \tag{6}$$

where $\chi(c_N)$ is equal to $e^{i2\pi/n}$, $n = 0, \pm 1, \ldots, \pm\lfloor \frac{N}{2} \rfloor$, and $\lfloor\rfloor$ is the rounding operator. Equation (6) can be rewritten as

$$\begin{bmatrix} u_{CB} \\ u_{CL} \\ u_T \\ u_R \\ u_I \end{bmatrix} = \begin{bmatrix} \chi(c_N) & 0 & 0 \\ I & 0 & 0 \\ 0 & \chi(c_N)e^{ik_x a_1} & 0 \\ 0 & I & 0 \\ 0 & 0 & I \end{bmatrix} \begin{bmatrix} u_{CL} \\ u_R \\ u_I \end{bmatrix}, \quad (7)$$

where I denotes the identity matrix. Equation (7) can be expressed as $u = Pu'$, where $u = \begin{bmatrix} u_{CB} \\ u_{CL} \\ u_T \\ u_R \\ u_I \end{bmatrix}$, $P = \begin{bmatrix} \chi(c_N) & 0 & 0 \\ I & 0 & 0 \\ 0 & \chi(c_N)e^{ik_x a_1} & 0 \\ 0 & I & 0 \\ 0 & 0 & I \end{bmatrix}$, $u' = \begin{bmatrix} u_{CL} \\ u_R \\ u_I \end{bmatrix}$. It is worth noting that the eigenmodes of solving for n equals $-m$ and n equals m are degenerate modes. Therefore, to acquire all band structures of the photonic crystal, $n = 0, 1, \ldots, \lfloor \frac{N}{2} \rfloor$ must be iterated $\lfloor \frac{N}{2} \rfloor + 1$ times. The boundary conditions obtained by combining the Bloch boundary conditions with rotation symmetry are referred to as rotational Bloch boundary conditions in this paper.

C. Finite Element Implementation

In FEM, the electric field can be expressed as an expansion of the basis functions; i.e., $E(x, y, z) = \sum u_j N_j$, where u_j is the DOF to be solved, N_j is the basis function. To solve the eigenfrequency of the photonic device with FEM, the discrete matrix $Au = \lambda Bu$ must be assembled by proper treatment of the vector wave equation [31], where $\lambda = k_0^2$, and A and B are the matrices with each matrix element given by

$$A_{ij} = \int \left(\nabla \times N_i \cdot \mu_r^{-1} \nabla \times N_j\right) \mathrm{d}S, \quad (8)$$

$$B_{ij} = \int \left(\epsilon_r N_i \cdot N_j\right) \mathrm{d}S. \quad (9)$$

As for a mirror symmetric photonic crystal, [Fig. 2(a)], the Bloch boundary conditions are applied to the T and B boundaries, while PEC/PMC will be applied to the M and L boundaries when using the mirror Bloch boundary conditions. Using rotational Bloch boundary conditions, it is possible to derive the final eigenvalue problem using Eq. (7) [32] to get

$$P^\dagger A P u' = \lambda P^\dagger B P u'. \quad (10)$$

Therefore, the eigenfrequency and electric field can be obtained by solving Eq. (10).

In summary, the significant features (i.e., symmetry, truncated domain, the numbers of DOFs and eigenvalue problems), of FEM with mirror Bloch boundary conditions (MBBC-FEM) and FEM with rotational Bloch boundary conditions (RBBC-FEM), are compared against FEM with standard Bloch boundary conditions (BBC-FEM), as tabulated in Table 1. The volumes of the truncated domain and DOFs of our proposed MBBC-FEM method can be reduced to at least 50% of their original values and reduced to $1/N$ of their original values for RBBC-FEM with c_N rotational symmetry. The proposed method increases the number of eigenvalue problems that must be solved, but it can still significantly improve the efficiency of solving the problems. Here is the rationale: The symmetry principle is used systematically to decompose the original problem into decoupled subtasks, which further grants that the overall solution time of the decomposed subtasks problems does have a simple linear relationship with the number of DOFs. Two numerical examples will be used in Section 3 to illustrate the computational efficiency of our proposed method.

Table 1. FEM Symmetry, Domain, DOFs, and Number of Eigenvalue Problems for Three Bloch Boundary Conditions

	BBC-FEM	MBBC-FEM	RBBC-FEM
Symmetry used in wave vector group	–	mirror symmetry	c_N rotational symmetry
Truncated domain	D	$D_v = D/2$	$D_N = D/N$
Number of DOFs	M	$M/2$	M/N
Number of eigenvalue problems	1	2	$\lfloor N/2 \rfloor + 1$

3. RESULTS AND DISCUSSIONS

To validate the universality and efficiency of the proposed method, we illustrate it through numerical examples of two-dimensional and three-dimensional photonic crystals. To facilitate the reader's understanding, we have chosen photonic crystals with the same symmetry as Fig. 2 for our computational example. The method presented in this paper is also applicable to any highly symmetric photonic crystal, including structures such as skewed lattices and honeycomb structures. All numerical results are obtained through COMSOL Multiphysics and MATLAB with homemade code. In this paper, the mesh density is denoted as S, and the maximum element size is set to $\frac{a}{S*n}$, where n is the refractive index, and a is the unit translation period length. The method of implementing rotating Bloch boundary conditions in COMSOL Multiphysics can be found in [7].

A. Two-Dimensional Photonic Crystal

To verify the universality of the proposed method, we compute the eigenmodes and band structures of a two-dimensional photonic crystal, which is shown in Fig. 3. The lattice vector of the photonic crystal is $R_n = \hat{x}an_1 + \hat{y}an_2$. The dielectric cylinder's diameter is $d = 0.4a$, the relative permittivity is $\epsilon_r = 2.25$, and the relative permeability is $\mu_r = 1$.

First, we compute the band structures of the two-dimensional photonic crystal using BBC-FEM and MBBC-FEM. The photonic crystal's wave vector group $G_0(k)$ along the highly symmetric line Γ-X-M-Γ is C_{2v} and mirror Bloch boundary conditions can be utilized to decrease the calculation domain. In light of the fact that Γ-X, X-M, and M-Γ are horizontal, vertical, and diagonal mirror planes, three different wave vector groups are used during the computational process. The reduction domain for different highly symmetric lines is distinct from each other. The band structure calculation results are shown in Fig. 3, where the blue line represents the TM mode calculated

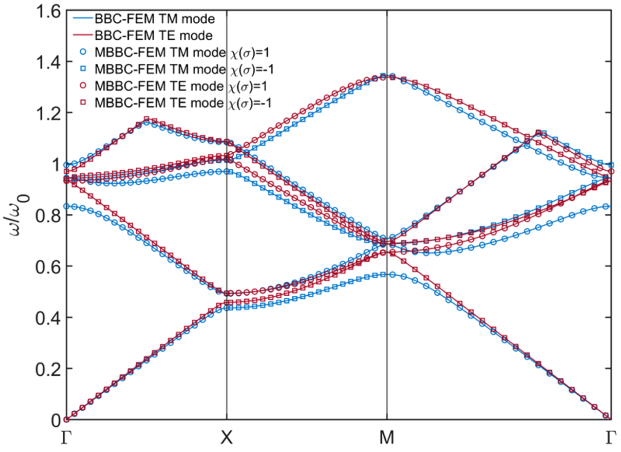

Fig. 3. Band structures of two-dimensional photonic crystals calculated by BBC-FEM and MBBC-FEM.

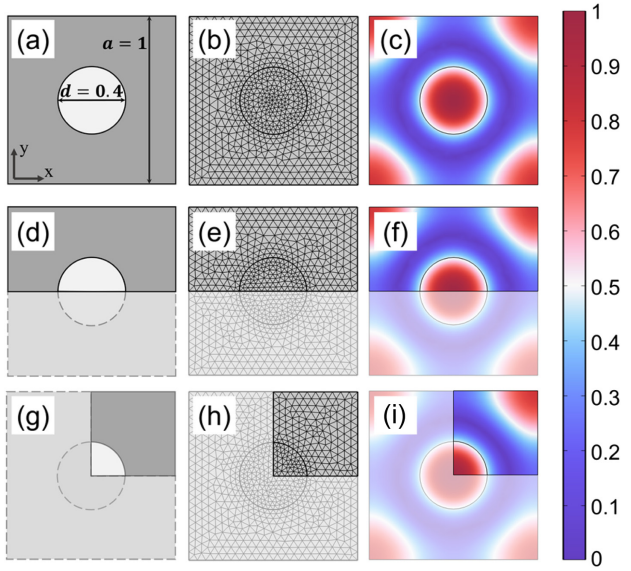

Fig. 4. Domain, mesh, and electric field intensity for different FEM methods. (a)–(c) Domain, mesh, and electric field intensity of BBC-FEM. (d)–(f) Domain, mesh, and electric field intensity of MBBC-FEM. (g)–(i) Domain, mesh, and electric field intensity of RBBC-FEM.

by BBC-FEM, the red line represents the TE mode calculated by BBC-FEM, the blue circles represent the TM mode calculated by MBBC-FEM with mirror symmetry, the blue squares represent the TM mode calculated by MBBC-FEM with mirror anti-symmetry, the red circles represent the TE mode calculated by MBBC-FEM with mirror symmetry, and the red squares represent the TE mode calculated by MBBC-FEM with mirror anti-symmetry. As mentioned in the Section 2, when using mirror symmetry, it is necessary to perform calculations twice to obtain the complete band structure of the photonic crystal. BBC-FEM and MBBC-FEM used the same mesh density, with a total of 1154 and 566 meshes and DOFs of 2381 and 1193, respectively. By using the calculation results of BBC-FEM as the reference value, the relative error with respect to the L2 norm for the two methods can be calculated as 1.4772e-3. It can be seen that our method is effective in calculating the band structures.

We calculate the eigenmodes at the Γ point for different methods and compare the electric field intensity distribution. The photonic crystal's wave vector group $G_0(k)$ is C_{4v} at the highly symmetric point Γ. When using mirror Bloch boundary conditions, the calculation domain can be reduced by half, as shown in Fig. 4(d). When using rotational Bloch boundary conditions, the calculation domain can be reduced to 1/4, as shown in Fig. 4(g). The TM mode's eigenfrequencies at the Γ point are calculated using BBC-FEM, MBBC-FEM, and RBBC-FEM with the same mesh density, and the meshes are shown in Figs. 4(b), 4(e), and 4(h), respectively. The corresponding electric field intensity distribution are shown in Figs. 4(c), 4(f), and 4(i), and the solved eigenfrequencies are 2.4992E8, 2.4999E8, and 2.4986E8, respectively. Figures 4(f) and 4(g) reconstruct the field distributions of the original domain from the truncated domain using Eq. (3) and render the restored field distribution transparent. The electric field intensity distribution has been normalized. It can be seen that our method can obtain the same results as BBC-FEM under the same mesh density.

To further analyze the computational accuracy and efficiency of the proposed method, the eigenfrequencies at the Γ point are calculated using different mesh densities. There is no analytical solution to the eigenfrequency problem of a 2D photonic crystal. Therefore, the eigenfrequencies obtained by BBC-FEM with $S = 200$ are used as the reference solution, and the result can be considered as the true solution due to the extremely dense mesh density. Additionally, to compare the results obtained by our method with those obtained by BBC-FEM, the relative error is defined as

$$\mathrm{Err} = \frac{1}{M}\sum_{i=1}^{M}\frac{\left|\omega_i^{2(\mathrm{FEM})} - \omega_i^{2(\mathrm{Refrence})}\right|}{\omega_i^{2(\mathrm{Refrence})}}, \tag{11}$$

where M is number of eigenmodes, and ω_i is the eigenfrequency of the i-th eigenmode.

Figure 5 shows the accuracy and normalized computation time of the TM and TE modes at different mesh densities for the structure of Fig. 4(a). The computation errors are calculated using the first 40 eigenmodes with eigenfrequencies greater than 1e8Hz to ensure that the correct modes are calculated. When using our method, multiple sub-eigenvalue problems must be computed as described in Section 2, and the computational time accounts for the cumulative sum of multiple calculations. All results are obtained using the same solver settings in COMSOL Multiphysics, ensuring that different methods use exactly the same eigenvalue solver. Aa shown in Fig. 5(a), under the same mesh density, BBC-FEM and MBBC-FEM have very similar computational accuracy, but RBBC-FEM has higher computational accuracy. This can be attributed to the stronger constraints imposed by RBBC-FEM compared to BBC-FEM and MBBC-FEM; namely that the electric field itself has rotational symmetry, which is implicitly satisfied in BBC-FEM and MBBC-FEM but strongly enforced as a boundary condition in RBBC-FEM. Figure 5(b) shows the computation time at different mesh densities. To compare the computational efficiency of different methods, we use the minimum calculation time for normalization and calculate the first 200 eigenmodes with eigenfrequencies greater than 1e8Hz. Because the computational time and DOFs are not linearly related, the

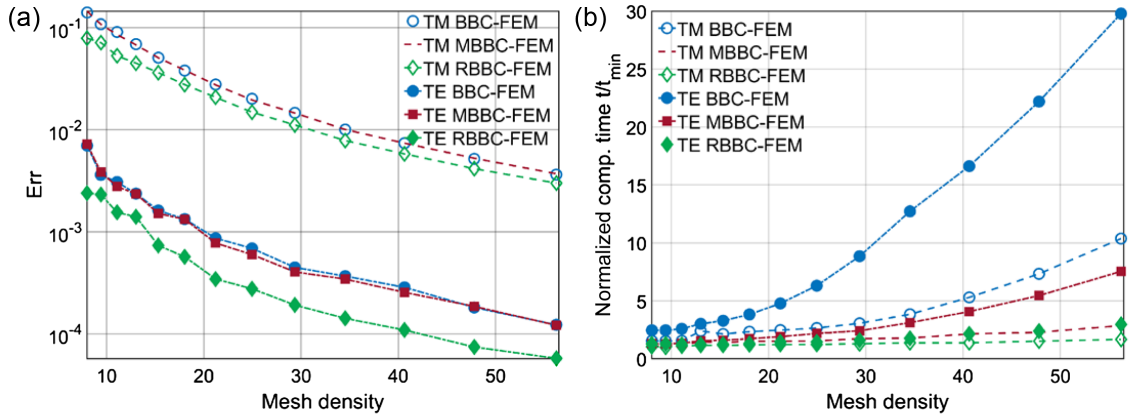

Fig. 5. Accuracy and normalized computational time of different FEM methods in relation to mesh density: (a) accuracy of different FEM methods and (b) normalized computational time of different FEM methods.

computational time increases exponentially with increasing mesh density. At $S = 56$, MBBC-FEM is nearly four times faster than BBC-FEM, and RBBC-FEM is nearly 10 times faster than BBC-FEM. Although RBBC-FEM is very effective, it is complex and imposes higher requirements on the symmetry of photonic devices, and $N > 2$ is usually only satisfied at a few highly symmetric points such as Γ. MBBC-FEM is more generally convenient and can usually be satisfied at highly symmetric lines, making it more suitable for calculating photonic band structures.

B. Three-Dimensional Photonic Crystal

Three-dimensional photonic crystals possess complex structures and demand sizeable computational resources for band structure calculations compared to two-dimensional counterparts. Therefore, the proposed method is advantageous in solving three-dimensional photonic crystals. To demonstrate the proposed method's efficiency, we provide an example of a face centered cubic photonic crystal structure in Fig. 6(a). The lattice vector, dielectric sphere's diameter, relative permittivity, and permeability are represented by $R_n = \hat{x}an_1 + \hat{y}an_2 + \hat{z}an_3$, $d = 0.6a$, $\epsilon_r = 12$, and $\mu_r = 1$, respectively. The wave vector group $G_0(k)$ on the ΓKWX plane is represented by $C_s(Ic_{2z})$, wherein the mirror Bloch boundary conditions can halve the calculation domain, as demonstrated in Fig. 6(b). This structure can also be computed using RBBC-FEM to simplify calculations, but the boundary conditions are not easily implemented in COMSOL Multiphysics. Therefore, we only validate the MBBC-FEM method proposed in this paper.

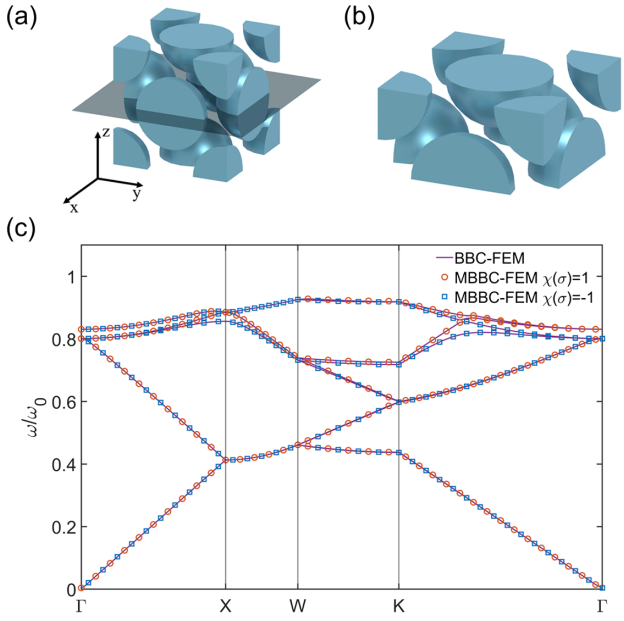

Fig. 6. Geometric structure and band structures: (a) geometric structure and domain of BBC-FEM, (b) domain of MBBC-FEM, and (c) band structures of a photonic crystal.

We calculate the band structures along the highly symmetric line Γ-X-W-K-Γ in the wave vector space using MBBC-FEM and BBC-FEM. In Fig. 6(c), the band structures indicate that the purple line corresponds to the band obtained through BBC-FEM, and the orange circles and the blue squares represent the band obtained through MBBC-FEM. The computed outcomes of both methods are proven to be identical. Table 2 presents the number of meshes, DOFs, computation time, memory usage, and error for both BBC-FEM and MBBC-FEM in calculating the band structures. The DOFs in the case of BBC-FEM are equal to 363082, whereas MBBC-FEM's DOFs are only half that of BBC-FEM. Due to the significant decrease in the DOFs, MBBC-FEM uses less than half of the memory occupied by BBC-FEM and solves the problem in approximately half of the time required by BBC-FEM. Meanwhile, the relative error between MBBC-FEM and BBC-FEM is 9.9906e-5. Thus, when computing the band structure of three-dimensional photonic crystals, utilizing our proposed method significantly reduces the solving time and memory usage and enhances the

Table 2. Computing Resources and Relative Errors for BBC-FEM and MBBC-FEM

	BBC-FEM	MBBC-FEM
Number of meshes	66715	32822
DOFs	81463	40754
CPU time	79.32 min	34.22 min
Memory	3.53 GB	1.67 GB
Error	–	9.9906e-5

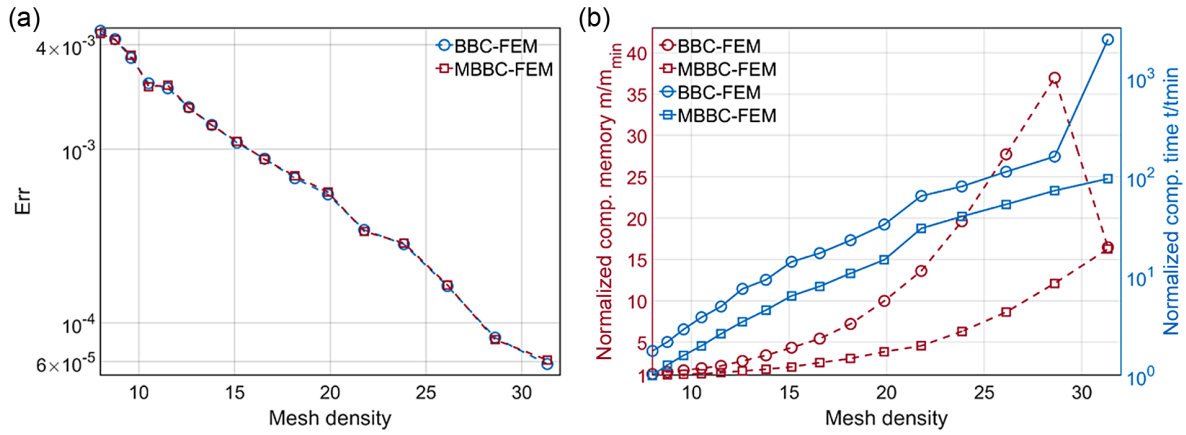

Fig. 7. Accuracy, normalized computational time, and normalized memory usage for BBC-FEM and MBBC-FEM in relation to mesh density. (a) Accuracy for BBC-FEM and MBBC-FEM. (b) Normalized computational time and normalized memory usage for BBC-FEM and MBBC-FEM. The right vertical axis depicts the normalized computational time. The left vertical axis depicts the normalized memory usage.

computational efficiency while maintaining computational accuracy.

We validate the computational accuracy and efficiency of our method by comparing the eigenfrequency problem with BBC-FEM at $k = [\frac{\pi}{2a}, \frac{\pi}{2a}, 0]^T$. The definition of error and mesh density S is the same as in Section 3.A. Figure 7 shows the accuracy, normalized computational time, and normalized memory usage of BBC-FEM and MBBC-FEM under different mesh densities for the same structure of Fig. 6(a). As in two dimensions, all results are obtained using the same solver settings in COMSOL Multiphysics. As shown in Fig. 7(a), under the same mesh density, BBC-FEM and MBBC-FEM have very similar computational accuracy. The results also are calculated using the first 40 eigenmodes with eigenfrequencies greater than 1e8Hz to ensure that the correct modes are calculated. Figure 7(b) shows the computation time and memory usage, which is normalized using the minimum time and minimum memory usage at different mesh densities. Unlike two-dimensional problems, memory usage in three-dimensional problems increases significantly. When the memory usage for solving does not reach the upper limit of computer memory, both the computational time and memory usage of MBBC-FEM are half of those of BBC-FEM. However, when the memory usage for solving reaches the upper limit of computer memory, the solution speed is severely limited. In Fig. 7(b), when the mesh density is greater than 30, the memory usage exceeds the computer limit, and the eigenvalue solver switches to using the external core for a solution. Although the memory usage decreases, the computation time increases by an order of magnitude. At this time, our method can significantly improve the solution efficiency.

4. CONCLUSION

We systematically study the application of a symmorphic space group in electromagnetic FEM via modified boundary conditions. We further illustrate our approach through the band structure and eigenmode calculations of photonic crystals at highly symmetric points or lines in the Brillouin zone. In contrast to the standard Bloch boundary conditions, our approach crucially relies on a symmetry group (i.e., a wave vector group), which guarantees that the original problems are decomposed into a series of decoupled problems with truncated computational domains. Therefore, our approach can indeed enhance the accuracy and efficiency by at least a factor of two in our test examples. For example, we provide a detailed procedure of how to implement these conditions of mirror and rotational symmetry operations, which are formulated into our generalized Bloch boundary conditions that are easily incorporated into the finite element implementation. The boundary conditions obtained in this paper can also be easily applied to other numerical methods, such as FDTD and the transfer matrix method, because these methods can obtain a similar eigen equation and impose constraints in a manner similar to FEM. In the calculation of the band structures of 3D photonic crystals, our proposed method significantly outperforms the conventional FEM approach in terms of memory usage and computational time when computer memory is limited. Considering the fundamental role of the group approach in optics as well as computational photonics, we believe that our work on the extension of standard Bloch boundary conditions to generalized Bloch boundary conditions based on the group theory is rather generic and provides insightful information about photonic bands and eigenmodes in a symmetric photonic structure. Therefore, our work might be useful in designing photonic devices with certain symmetries, or in topological photonics where symmetry plays a relevant role.

Funding. Hubei Province Key Research and Development Program Projects (2023DJC172); National Key Research and Development Program of China (2021YFB2800303); National Natural Science Foundation of China (12274161); Innovation Project of Optics Valley Laboratory.

Disclosures. The authors declare no conflicts of interest.

Data availability. Data underlying the results presented in this paper are not publicly available at this time but may be obtained from the authors upon reasonable request.

REFERENCES

1. K. Chen, J. Song, and T. Kamgaing, "Metal grip grating on grounded dielectric slab and PEC/PMC shielded interconnect: modal relationships," Appl. Comput. Electromagn. Soc. J. **29**, 828–836 (2014).

2. R. Otin, J. Verpoorte, and H. Schippers, "Finite element model for the computation of the transfer impedance of cable shields," IEEE Trans. Electromagn. Compat. **53**, 950–958 (2011).
3. H. P. Uranus, J. Pangaribuan, and M. Gracio A. R., "Theoretical characterization of a commercial large mode area–endlessly single mode photonic crystal fiber," in *IEEE PhotonicsGlobal@Singapore* (2008), pp. 1–4.
4. P. Nyakas, "Full-vectorial three-dimensional finite element optical simulation of vertical-cavity surface-emitting lasers," J. Lightwave Technol. **25**, 2427–2434 (2007).
5. K. Z. Aghaie, S. Fan, and M. J. F. Digonnet, "Birefringence analysis of photonic-bandgap fibers using the hexagonal Yee's cell," IEEE J. Quantum Electron. **46**, 920–930 (2010).
6. I. Andonegui and A. J. Garcia-Adeva, "The finite element method applied to the study of two-dimensional photonic crystals and resonant cavities," Opt. Express **21**, 4072–4092 (2013).
7. Z. Wang, J. Wang, L. Liu, *et al.*, "Rotational Bloch boundary conditions and the finite-element implementation in photonic devices," Photonics **10**, 691 (2023).
8. G. Garcia-Contreras, J. Córcoles, and J. A. Ruiz-Cruz, "Degeneracy-discriminating modal FEM computation in higher order rotationally symmetric waveguides," IEEE Trans. Antennas Propag. **69**, 8003–8008 (2021).
9. G. Garcia-Contreras, J. Córcoles, and J. A. Ruiz-Cruz, "Rigorous modal characterization of first- and second-order symmetric waveguides using specular periodic boundary conditions in 2D-FEM," IEEE Trans. Antennas Propag. **70**, 10800–10810 (2022).
10. A. Nicolet, S. Guenneau, C. Geuzaine, *et al.*, "Modelling of electromagnetic waves in periodic media with finite elements," J. Comput. Appl. Math. **168**, 321–329 (2004).
11. A. A. Tavallaee and J. P. Webb, "Finite-element modeling of evanescent modes in the stopband of periodic structures," IEEE Trans. Magn. **44**, 1358–1361 (2008).
12. N. Sukumar and J. E. Pask, "Classical and enriched finite element formulations for Bloch-periodic boundary conditions," Int. J. Numer. Methods Eng. **77**, 1121–1138 (2009).
13. B. P. Hiett, J. M. Generowicz, S. J. Cox, *et al.*, "Application of finite element methods to photonic crystal modelling," IEE Proc. Sci. Meas. Technol. **149**, 293–296 (2002).
14. G. Parisi, P. Zilio, and F. Romanato, "Complex Bloch-modes calculation of plasmonic crystal slabs by means of finite elements method," Opt. Express **20**, 16690–16703 (2012).
15. D. Boffi, M. Conforti, and L. Gastaldi, "Modified edge finite elements for photonic crystals," Numer. Math. **105**, 249–266 (2006).
16. J. D. Joannopoulos, S. G. Johnson, J. N. Winn, *et al.*, "Photonic crystals: molding the flow of light," in *Photonic Crystals*, 2nd ed. (Princeton University, 2011).
17. J. D. Joannopoulos, P. R. Villeneuve, and S. Fan, "Photonic crystals," Solid State Commun. **102**, 165–173 (1997).
18. D. C. Marinica, A. G. Borisov, and S. V. Shabanov, "Bound states in the continuum in photonics," Phys. Rev. Lett. **100**, 183902 (2008).
19. Y. Chen, H. Deng, X. Sha, *et al.*, "Observation of intrinsic chiral bound states in the continuum," Nature **613**, 474–478 (2023).
20. Y. Yang, C. Peng, Y. Liang, *et al.*, "Analytical perspective for bound states in the continuum in photonic crystal slabs," Phys. Rev. Lett. **113**, 037401 (2014).
21. Z. Liu, X. Li, C. Chen, *et al.*, "Bound states in the continuum in asymmetric one-dimensional photonic crystal systems guided by anisotropy," Opt. Express **31**, 8384–8392 (2023).
22. S. Dai, P. Hu, and D. Han, "Near-field analysis of bound states in the continuum in photonic crystal slabs," Opt. Express **28**, 16288–16297 (2020).
23. Y. Lei, X.-W. Luo, and S. Zhang, "Second-order topological insulator in periodically driven optical lattices," Opt. Express **30**, 24048–24061 (2022).
24. C. Jiang, Y. Song, X. Li, *et al.*, "Photonic Möbius topological insulator from projective symmetry in multiorbital waveguides," Opt. Lett. **48**, 2337–2340 (2023).
25. J.-Y. Huang, X.-F. Xu, H. Zhang, *et al.*, "Topological boundary states of two-dimensional restricted isosceles triangular photonic crystals," Appl. Opt. **61**, 1254–1260 (2022).
26. W. Hu, J. Hu, S. Wen, *et al.*, "Dynamically reconfigurable topological states in photonic crystals with liquid crystals," Opt. Lett. **46**, 2589–2592 (2021).
27. H. Yoshimi, T. Yamaguchi, Y. Ota, *et al.*, "Slow light waveguides in topological valley photonic crystals," Opt. Lett. **45**, 2648–2651 (2020).
28. J.-W. Dong, X.-D. Chen, H. Zhu, *et al.*, "Valley photonic crystals for control of spin and topology," Nat. Mater. **16**, 298–302 (2017).
29. S. Iwamoto, Y. Ota, and Y. Arakawa, "Recent progress in topological waveguides and nanocavities in a semiconductor photonic crystal platform [Invited]," Opt. Mater. Express **11**, 319–337 (2021).
30. V. Heine, "Group theory: application to the physics of condensed matter," Phys. Today **61**, 57–58 (2008).
31. G. Pelosi, R. Coccioli, and S. Selleri, *Quick Finite Elements for Electromagnetic Waves* (Artech House, 2009).
32. J.-M. Jin, *The Finite Element Method in Electromagnetics* (Wiley, 2015).